

MIT Open Access Articles

Experimental Measurement of Overpotential Sources during Anodic Gas Evolution in Aqueous and Molten Salt Systems

The MIT Faculty has made this article openly available. **Please share** how this access benefits you. Your story matters.

Citation: Chmielowiec, Brian John et al. "Experimental Measurement of Overpotential Sources during Anodic Gas Evolution in Aqueous and Molten Salt Systems." *Journal of The Electrochemical Society* 166, 10 (June 2019): E323. © 2019 The Author(s)

As Published: <http://dx.doi.org/10.1149/2.1001910jes>

Publisher: The Electrochemical Society

Persistent URL: <https://hdl.handle.net/1721.1/131147>

Version: Final published version: final published article, as it appeared in a journal, conference proceedings, or other formally published context

Terms of use: Creative Commons Attribution-NonCommercial-NoDerivs License





Experimental Measurement of Overpotential Sources during Anodic Gas Evolution in Aqueous and Molten Salt Systems

Brian Chmielowiec,¹ Tatsuki Fujimura,² Tomohiro Otani,² Kiego Aoyama,³
Toshiyuki Nohira,^{1b,3,*} Takayuki Homma,^{1b,2,*} Yasuhiro Fukunaka,^{2,*}
and Antoine Allanore^{1b,*,z}

¹Department of Materials Science and Engineering, Massachusetts Institute of Technology, Cambridge, Massachusetts 02139, USA

²Department of Applied Chemistry, Waseda University, Okubo, Shinjuku, Tokyo 169-8555, Japan

³Institute of Advanced Energy, Kyoto University, Gokasho, Uji, Kyoto 611-001, Japan

Current interrupt and galvanostatic EIS techniques were utilized in a complementary fashion to characterize the different sources of overpotential during anodic gas evolution. Room temperature anodic evolution of oxygen at a nickel working electrode in aqueous potassium hydroxide and the high temperature (348°C) anodic evolution of chlorine at a glassy carbon working electrode in molten (LiCl)_{57.5}-(KCl)_{13.3}-(CsCl)_{29.2} were investigated. Combining of the two techniques enables to separate the total measured overpotential into its ohmic, charge transfer, and mass transfer components. Potential decay curves indicated that natural convection (due to both bubble evolution and density driven flow) was a major driving force in reestablishing equilibrium conditions at the working electrode surface. During oxygen evolution, charge transfer resistance dominated the total overpotential at low current densities, but as the current density approached ~100 mA/cm², mass transfer overpotentials and ohmic overpotential became non-negligible. The mass transfer overpotential during chlorine evolution was found to be half that found during oxygen evolution.

© The Author(s) 2019. Published by ECS. This is an open access article distributed under the terms of the Creative Commons Attribution Non-Commercial No Derivatives 4.0 License (CC BY-NC-ND, <http://creativecommons.org/licenses/by-nc-nd/4.0/>), which permits non-commercial reuse, distribution, and reproduction in any medium, provided the original work is not changed in any way and is properly cited. For permission for commercial reuse, please email: oa@electrochem.org. [DOI: 10.1149/2.1001910jes]



Manuscript submitted April 2, 2019; revised manuscript received June 4, 2019. Published June 28, 2019.

With the transition toward carbon-free production of electric power, there is an opportunity for the electrification of the production of fuels, chemicals, and structural materials. Electrolysis is one potential process to generate renewable fuel (e.g. water splitting for hydrogen) and structural materials (steel, copper, or light metals electro-winning, for example in molten chlorides, oxides, or sulfides).

A common feature to all these electrolytic processes is the evolution of gas at either one or both electrodes - oxygen and hydrogen in water electrolysis, chlorine in molten chloride electrolysis, oxygen in molten oxide electrolysis, and sulfur in molten sulfide electrolysis. Gas evolution poses both advantages and challenges to the electrochemical engineer. Enhanced convection due to the rise of gas bubbles increases mass transfer to the electrode surface, enabling higher current density, which enables higher productivity.¹⁻³ On the other hand, a steady-state bubble layer restricts the current path to the electrode surface. The two-phase gas/liquid electrolyte thus has an increased effective resistance. Additionally, bubbles that adhere to the electrode shield its surface, thereby reducing the electrochemically active surface area and locally increasing the actual current density passing through an electrode.

These last two effects can give rise to significant ohmic losses and (at low temperature) charge transfer overpotentials that are detrimental to the energy efficiency of such electrochemical cells. Bubble evolution under industrially relevant current density regimes (>~100 mA/cm²) thus represents a unique combination of ohmic, kinetic, and mass transfer overpotentials. For example, in the Hall-Héroult cell for aluminum production, Haupin⁴ estimated the overpotential due to charge transfer kinetics is around 250 mV, while nearly 1500 mV overpotential is due to bulk solution resistance. Estimates of 250 mV overpotential due to the bubble layer resistance and ~100 mV due to concentration polarization at the two electrodes are reported. The deconvolution of the measured cell voltage (difference of potential) into these individual overpotential contributions is a challenging, but necessary task to understand the factors limiting the performance of a given electrochemical cell and optimize its design.

The Current Interrupt (CI) method has classically been used to measure solution resistance.⁵ Electrochemical Impedance Spectroscopy

(EIS) gives access to both the solution resistance and (when present) charge transfer resistance. This work aims to use a combination of these techniques to distinguish and quantify the overpotentials due to ohmic resistance, charge transfer resistance, and mass transfer resistance in electrochemical cells evolving oxygen or chlorine at the anode surface. The oxygen evolution reaction (OER) and the chlorine evolution reaction (CER) were chosen as case studies due to their industrial relevance and due to the similarity in their anticipated overpotential dependences save for one key difference: charge transfer resistance.

The overpotential dependencies for OER and CER are anticipated to be similar, except for the presence of significant charge transfer resistance during room temperature OER. These dependencies are outlined below. Equations 1a and 1b are the target anodic gas evolution reactions in alkaline electrolysis and molten chloride electrolysis, respectively:

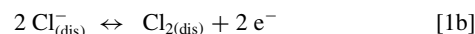
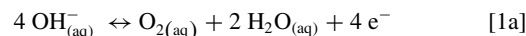


Table I below shows the corresponding electrochemical definitions (Equations 2 to 5, see List of Symbols for definition), and their specific application to OER and CER reactions is provided in their respective columns. The subscripts on the overpotential terms (ct, and mt) correspond, respectively, to charge transfer and mass transfer, and iR_s represents ohmic resistance.

For the oxygen evolution reaction (OER), Reaction 1a directly involves water molecules. Accordingly, the activity of the water molecules is present in the Nernst equation (Equation 2). However, Balej⁶ measured the dependence of water activity on the concentration of potassium hydroxide and found that it decreases by less than 25% when the potassium hydroxide concentration is as large as 5 mol/kg H₂O. Thus, the change in activity of water due to a depleted concentration of hydroxide ions at the electrode surface during electrolysis is not expected to impact the potential by more than 5 mV and can safely be ignored in even moderately concentrated basic solutions.

The chlorine evolution Reaction 1b at an inert anode such as glassy carbon⁷ in molten halide systems is simpler both conceptually and practically because only chloride species are involved in the half reaction, and due to the higher temperature, the charge transfer

*Electrochemical Society Member.

^zE-mail: allanore@mit.edu

Table I. Equation 2 defines the equilibrium thermodynamic potential (E_{eq} , Nernst) where $\prod_i a_{i,eq}^{v_i}$ accounts for the product of species activities ($a_{i,eq}$) raised to their respective stoichiometric coefficients, (v_i). Equation 3 expresses the applied electrochemical potential under current flow where $\sum_i \eta_i$ accounts for all the overpotential contributions. Equation 4 provides the mass transfer contribution and Equation 5 the total overpotential. The Nernst potential has been explicitly expanded into the standard potential (E^0) and the individual activities of the reactants and products using the appropriate stoichiometric coefficients, and the main contributions to total overpotential for each reaction are explicitly expanded, where iR_s is the overpotential inherited from the overall ohmic resistance and η_{ct} is the overpotential required for charge transfer as predicted by the Butler Volmer equation.

Definitions	OER 1a	CER 1b
(2) $E_{eq} = E^0 - \frac{RT}{n_e F} \ln \prod_i a_{i,eq}^{v_i}$	$n_e = 4 \nu_{O_2} = -1, \nu_{H_2O} = -2, \nu_{OH^-} = 4$	$n_e = 2 \nu_{Cl_2} = -1, \nu_{Cl^-} = 2$
(3) $E_{app} = E^0 - \frac{RT}{n_e F} \ln \prod_i a_{i,app}^{v_i} + \sum_i \eta_i$		
(4) $\eta_{mt} = -\frac{RT}{n_e F} \ln \prod_i \left(\frac{a_{i,app}}{a_{i,eq}} \right)^{v_i}$	$\eta_{mt} = -\frac{RT}{4F} \ln \left(\frac{a_{OH_{app}}}{a_{OH_{eq}}} \right)^4 - \frac{RT}{4F} \ln \left(\frac{a_{O_2,app}}{a_{O_2,eq}} \right)^{-1} - \left(\frac{RT}{4F} \ln \left(\frac{a_{H_2O,app}}{a_{H_2O,eq}} \right)^{-2} \approx 0 \right)$	$\eta_{mt} = -\frac{RT}{2F} \ln \left(\frac{a_{Cl_{app}}}{a_{Cl_{eq}}} \right)^2 - \frac{RT}{2F} \ln \left(\frac{a_{Cl_2,app}}{a_{Cl_2,eq}} \right)^{-1}$
(5) $\eta_{tot} = E_{app} - E_{eq}$	$\eta_{tot}^{(1a)} = iR_s + \eta_{ct} + \eta_{mt}$	$\eta_{tot}^{(1b)} = iR_s + \eta_{mt}$

overpotential becomes negligibly small. In particular, for the relatively simple mixtures of alkali chlorides, the only electroactive chloride species is indeed Cl^- .⁸ The final row in Table I highlights the expected main contributors to total overpotential, with the mass transfer overpotential (η_{mt}) explicitly expanded in the row above. The quantities $\frac{RT}{4F} \ln \left(\frac{a_{O_2,app}}{a_{O_2,eq}} \right)$ and $\frac{RT}{2F} \ln \left(\frac{a_{Cl_2,app}}{a_{Cl_2,eq}} \right)$ have commonly been described as the supersaturation overpotential for gas evolution because the dissolved concentration of gas next to the electrode surface is anticipated to far exceed its equilibrium value found in the bulk solution.⁹⁻¹³

The only phenomenological difference between the two reactions is charge transfer resistance which is present during OER, due to the low temperature of the alkaline solutions, but hardly noticeable during CER conducted in molten halides at a relatively higher temperature.^{14,15} By quantifying the individual contributions of ohmic, kinetic, and mass transfer limitations to the total cell overpotential, the electrochemical engineer can then identify the best path to lower the cell voltage by fine tuning key properties such as electrode design, wettability, density of gas nucleation centers, etc.

Previous studies by Fukunaka and coworkers measured the ohmic overpotential and mass transfer overpotential associated with supersaturation of H_2 evolved at Pt electrodes utilizing the CI technique.^{9,16,17} During galvanostatic electrolysis, the working electrode potential tends toward a steady-state value determined by the standard reduction potential (thermodynamics), exchange current density (charge transfer kinetics), concentration gradients (mass transport), and solution conductivity (ohmic resistance). In the case of bubble evolution, the nucleation, growth, and departure of bubbles perturb the active electrode area and local concentration gradients and thus can cause small fluctuations around this steady-state value of electrode potential. Figure 1 shows an equivalent circuit to model an electrochemical half-cell alongside a representative potential decay curve (PDC) when the current is interrupted.

Upon the cessation of current, the ohmic drop (η_{iR}) across R_s (representing ohmic resistance of both the bulk electrolyte and possible

bubble layer) immediately disappears. However, at this point, concentration gradients still exist – the activity of reactants and products at the electrode surface are lower and higher, respectively, than they were under open circuit conditions. Thus, the electrode potential is still above (in the case of an anode) or below (in the case of a cathode) the open circuit value. The measured potential decays back to the open circuit value as reactant and product concentrations return to their bulk values, first as the electrochemical double layer (C_{dl}) discharges, then followed by mass transport of products away from (and reactants to) the electrode surface. In the case of low charge transfer resistance (a small η_{ct} value), not much overvoltage was required to achieve the applied current density and the potential decay is small. The opposite is true for large charge transfer resistances. By far the slowest process is the diffusion of species to/away from the electrode surface to reestablish the bulk concentrations everywhere in the system (represented as Z_w , a Warburg-like impedance in Figure 1). In the limiting case of H_2 evolution on Pt, previous researchers chose to neglect η_{ct} due to the large exchange current density ($\sim 1 \text{ mA/cm}^2$) of proton reduction on Pt. They also chose to neglect the mass transfer overpotential for protons, presumably due to the high mobility of H^+ in solution.^{9,18} Herein the situation for the oxygen evolution reaction in alkaline electrolyte is different, as it is reported to be kinetically slow (exchange current density $j_0 \sim 10^{-7} \text{ mA/cm}^2$ on Ni)¹⁹ and to involve the transport of hydroxide ions (diffusivity at infinite dilution $\sim 5.3 \cdot 10^{-5} \text{ cm}^2 \text{ s}^{-1}$) rather than protons (diffusivity at infinite dilution $\sim 9.3 \cdot 10^{-5} \text{ cm}^2 \text{ s}^{-1}$).²⁰ Furthermore, oxygen bubbles have been observed to stick to the electrode surface, decreasing the active surface area.¹⁷ Therefore, the analysis of the potential decay curve for OER requires that ohmic, kinetic, and mass transfer overpotentials not be neglected.

Experimental

Materials and methods.—KOH (Kanto Chemicals, UGR grade) solutions with concentrations of 3.6M and 0.36M were used for the study of the oxygen evolution reaction. Gold and nickel foils ($1 \text{ cm} \times 1 \text{ cm} \times 0.3 \text{ mm}$, Nilaco Corp, 99.95%) were used as working electrodes. Preliminary results for OER at the Au electrode indicated competing electrochemical reactions (see supplementary section, S.1) so further studies with this material were not performed. A Ni foil ($1 \text{ cm} \times 3 \text{ cm} \times 0.3 \text{ mm}$, Nilaco Corp, 99.95%) was used as the counter electrode. The cell container was made from acrylic sheets that were laser cut and epoxied together. Figure 2 shows the electrochemical cells with key dimensions listed. A nickel mesh was positioned 1 cm away from the counter electrode to prevent mixing of hydrogen gas bubbles generated at the cathode during the electrolysis. A Ni wire (1 mm diameter, Alfa Aesar, 99.99% purity) was used as a quasi-reference electrode and positioned 5 mm away from the center of the working electrode. A conventional Hg/HgO reference electrode was initially used, but it

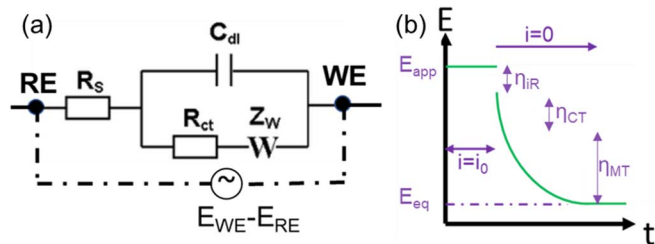


Figure 1. (a) Equivalent circuit model of half an electrochemical cell. (b) A typical potential decay curve following the cessation of an applied steady state current. The potential decays as the double layer discharges and the surface concentrations return to the bulk values.

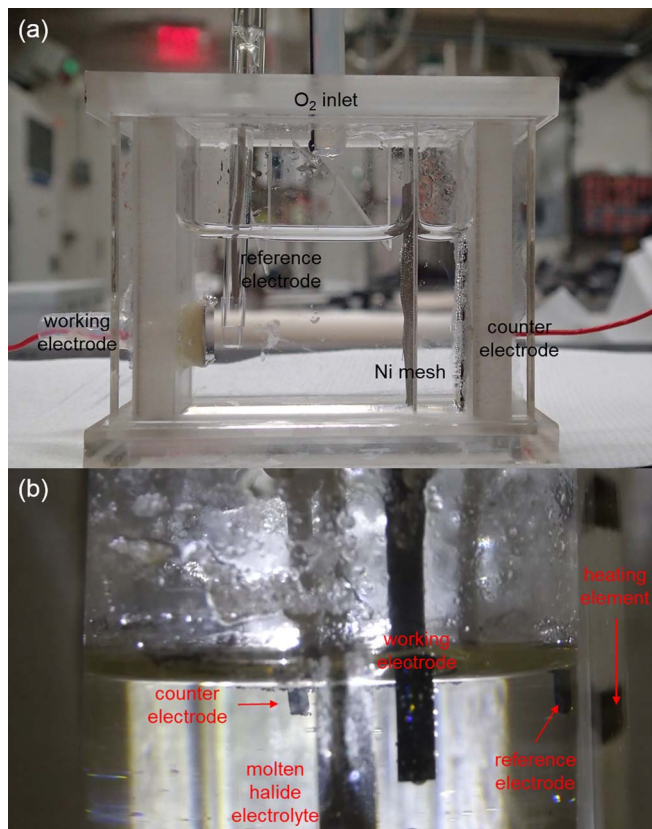


Figure 2. (a) Electrochemical cell used for Current Interrupt and Electrochemical Impedance Spectroscopy measurements in aqueous systems. The electrolyte occupies a volume of 13mm (W) \times 50mm (L) \times 30mm (H). The reference electrode is positioned \sim 5mm away from the working electrode surface, and a Ni mesh is positioned 1 cm away from the counter electrode to minimize the spread of H₂ bubbles toward the working electrode. (b) Electrochemical cell used for Current Interrupt measurements in molten salt. The diameter of the Pyrex crucible was 54mm. The furnace was kept at 348.1°C \pm 0.2°C.

was determined that the impedance of this reference electrode was too large for the time resolution needed.

For the molten salt system, reagent-grade LiCl (Wako Pure Chemical Co., Ltd., 99.0%), KCl (Wako Pure Chemical Co., Ltd., 99.5%), and CsCl (Wako Pure Chemical Co., Ltd., 99.0%) were dried under vacuum for more than 24 h at 200°C. A eutectic mixture (LiCl)_{57.5} - (KCl)_{13.3} - (CsCl)_{29.2} was mixed together in an ultra-dry chamber followed by melting in a resistive heating furnace inside of an argon purged glove box. A 54mm diameter flat bottomed closed one end tube served as the crucible. The working electrode was a glassy carbon rod (4mm diameter, Tokai Carbon Co., Ltd.). The counter electrode was a Ni wire (1mm diameter, Nilaco Corp, 99.95% purity), and the reference electrode was a two-phase Li-Al alloy whose preparation has been described elsewhere.⁷ This alloy has been shown to maintain a stable potential vs Li/Li⁺ for more than 12 hours.⁷

Electrochemical measurements.—Cyclic voltammograms were performed to pretreat the Ni surface. Reproducible current peaks were found corresponding to Ni^{2+/3+} redox reactions at the surface. Galvanostatic measurements and preliminary current interrupt measurements were carried out using a potentiostat/galvanostat (HZ-7000, Hokuto Denko) at a temperature of \sim 23°C to study OER. An HZ-3000 (Hokuto Denko) potentiostat/galvanostat was used to conduct current interrupt measurements in the molten halide system at a temperature of 348°C. EIS and current interrupt methods were used in subsequent aqueous experiments using a Reference 3000 (Gamry) potentiostat/galvanostat. The data sampling rate was 50kHz for the current interrupt measurements. Due to the insufficiently high sam-

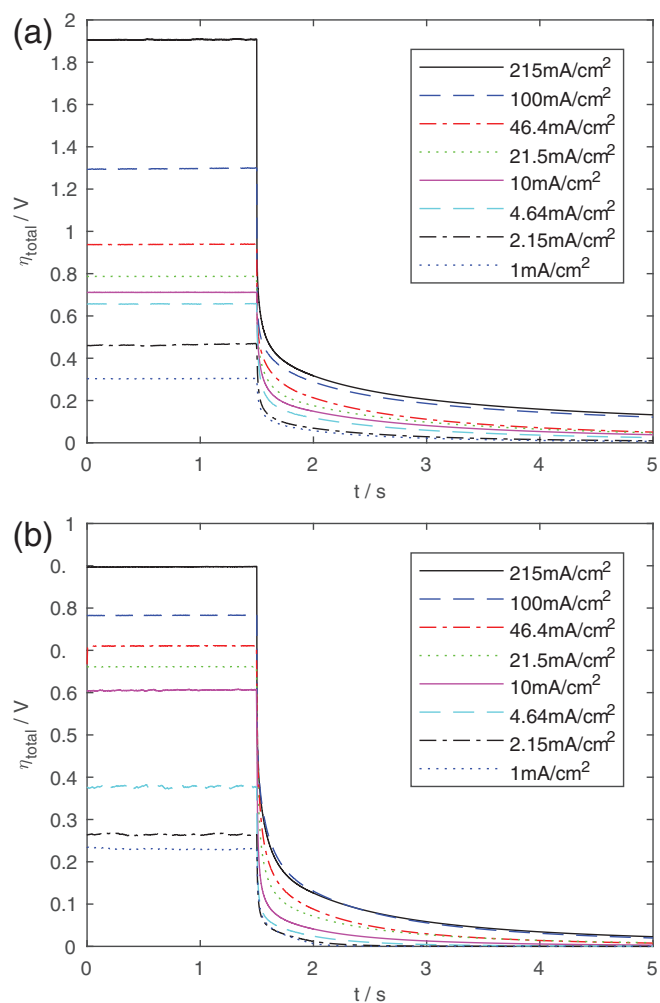


Figure 3. Variation of the total overpotential ($\eta_{tot} = E_{app} - E_{eq}$) with time after the oxygen evolution reaction at various current densities is interrupted in (a) 0.36M and (b) 3.6M KOH.

pling rate, extrapolation of the potential decay curve was needed to accurately determine the ohmic overpotential. More details about this method are available in the Supplementary Section. The electrode was held at fixed current density (1, 2.15, 4.64, 10, 21.5, 46.4, 100, 215mA/cm²) for 5 minutes before interrupting the current for OER. For CER, current densities of 464 and 1000mA/cm² were also used. Galvanostatic EIS was performed at the same fixed current density as the CI measurements while sweeping the AC perturbation from 100kHz to 1Hz for current densities above 2.15mA/cm² and 100kHz to 0.1Hz for current densities of 1 to 2.15mA/cm². The amplitude of perturbation was 0.1mA RMS for DC currents of 1 to 4.64mA/cm² and 1mA RMS for DC currents of 10 to 215mA/cm².

Results

Current interrupt and EIS results.—OER on nickel.—CI measurements were performed using the standard chronopotentiometry scripts written for each potentiostat with current cutoff using the electrochemical cells shown in Figure 2 to measure the total overpotential. Figure 3 shows the potential decay curve for a Ni working electrode in two KOH solutions of differing ionic strength. It must be noted that the absolute value of the ohmic overpotential should not be directly compared between the two electrolyte systems because the position of the reference electrode was only reproducible within \sim 1mm after the electrochemical cell was cleaned and electrolyte exchanged. However for measurements made within a single electrolyte system, the

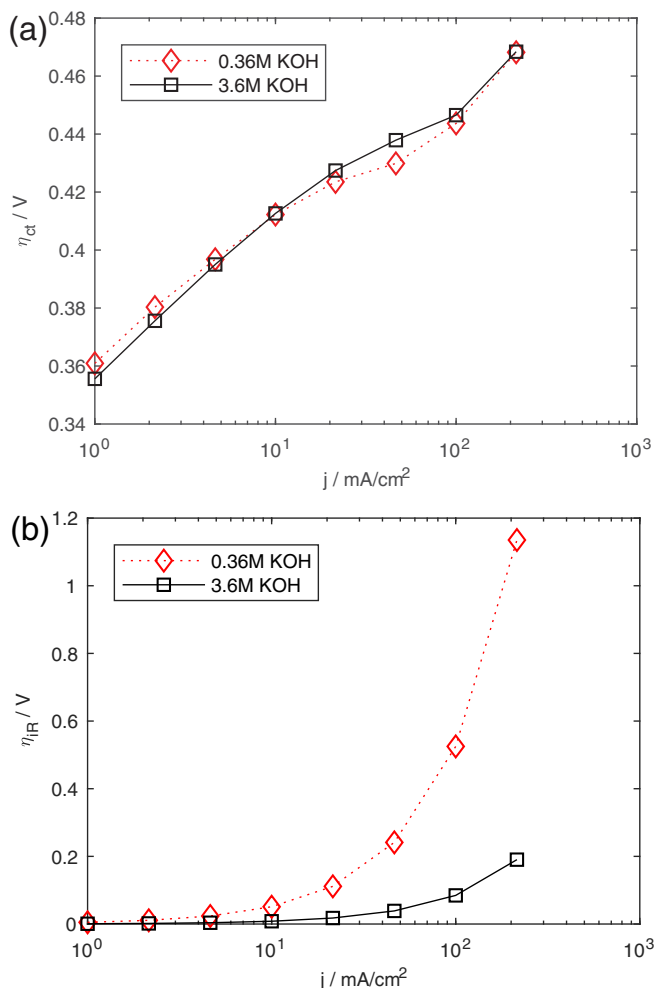


Figure 4. (a) Variation of the charge transfer overpotential for OER on Ni and (b) variation of the solution resistance overpotential for OER on Ni as measured by galvanostatic EIS. The charge transfer resistance measured during EIS was used in conjunction with the Butler Volmer equation to calculate the charge transfer overpotential.

reference electrode position was fixed so changes in the measured solution resistance can be attributed solely to bubble evolution.

Galvanostatic EIS was performed on a Ni electrode at current densities of 1, 2.15, 4.64, 10, 21.5, 46.4, 100, and 215 mA/cm² with frequency range studied of 200kHz to 1Hz (down to 0.1Hz for $j = 1$ and 2.15mA/cm²). Warburg-type impedance was not observed in the investigated frequency range. In all cases, the solution resistance, as determined by the intercept of the real impedance axis at high frequency, increased with increasing current density. The spectra recorded with a Ni working electrode varied smoothly with increasing current density: solution resistance increased and polarization resistance decreased with increasing current density. 3.6M KOH exhibited a lower solution resistance (is more conductive) with similar polarization resistance at a given current density compared to 0.36M KOH case. The charge transfer resistance was determined by extrapolating the Nyquist curve to the low frequency real impedance intercept and subtracting off the solution resistance previously discussed. It is found in Figure 4. It is clear from Figure 4 that the solution resistance and charge transfer overpotentials depend in a non-linear fashion with the applied current density.

Figure 5 presents the measured ohmic overpotential during OER in 3.6M KOH (represented as crosses) and compares it with the predicted ohmic overpotential from extrapolating η_{IR} for constant R_s (solid line). The latter is indicative of the ohmic contribution in absence of the bub-

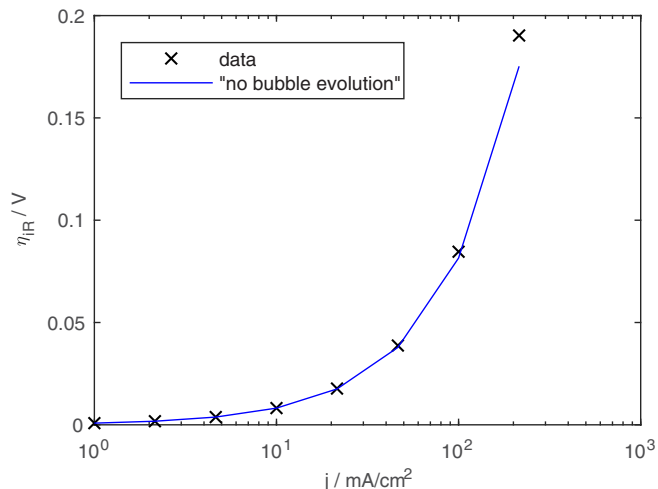


Figure 5. Variation of the ohmic overpotential measured (discrete data points) and extrapolated from R_s @ $j = 0$ mA/cm² (solid line) with current density during OER in 3.6M KOH.

ble layer on gas evolution, and proves valid up to ~ 100 mA/cm², above which an appreciable discrepancy with the actual ohmic resistance is observed.

Having determined the ohmic and charge transfer overpotentials, it is possible to subtract these contributions from the total overpotential to evaluate the mass transfer overpotential, as presented in Figure 6 in 0.36M and 3.6M KOH electrolytes. Virtually no mass transfer limitation is observed for current densities below 10 mA/cm².

CER on glassy carbon.—The current interrupt technique was applied in the eutectic chloride melt at a temperature of 348°C. The open circuit potential was measured with respect to an Al-Li two-phase reference electrode. To help saturate the solution with gas, Cl₂ gas was evolved at the working electrode for several minutes before starting the measurements at lower current density. As shown in Figure 7, the overpotential relaxes back to 0V much more quickly than the low temperature OER case. At the same current density, larger bubbles were found to adhere to the surface of the glassy carbon electrode than at the surface of the Ni electrode after the cessation of current.

EIS was not performed in the molten salt case so only CI results were used to calculate the ohmic and mass transfer overpotentials in this system. These overpotentials are shown in Figure 8.

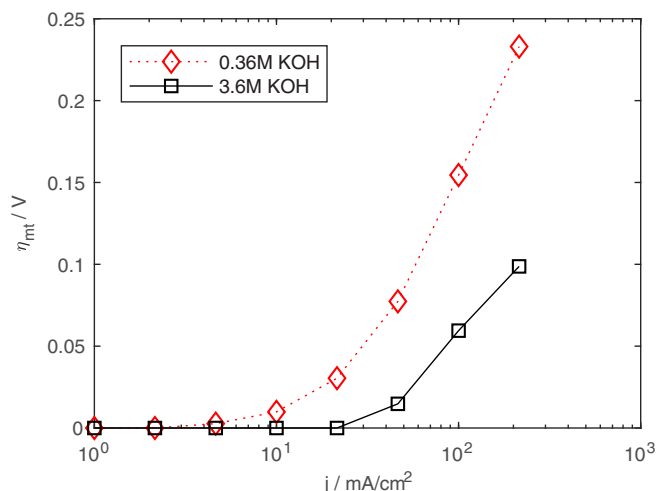


Figure 6. Variation of the mass transfer contribution to overpotential during OER on Ni working electrode as a function of current density.

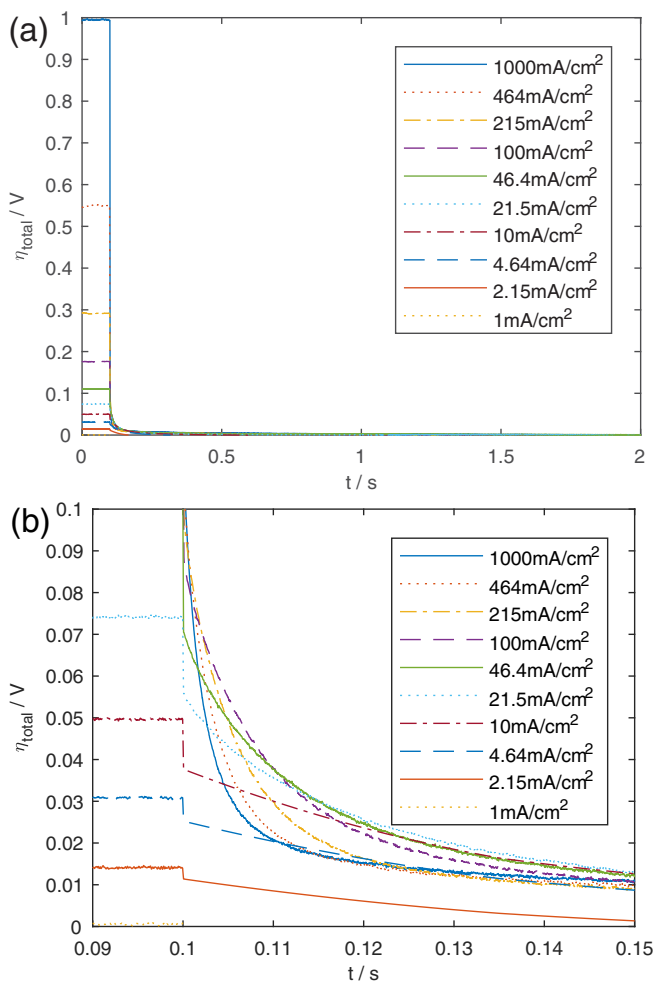


Figure 7. (a) Variation of the total overpotential with time for chlorine evolution reaction on glassy carbon at various current densities. (b) Inset of plot (a) highlighting the swift return of the overpotential to 0V roughly 50ms after the current interrupt.

Discussion

The rate at which the potential decays in Figure 3 varies between the two concentrations of KOH electrolytes. The more concentrated electrolyte (3.6M KOH) has the slowest rate of decrease back to equilibrium conditions. Considering that this system should have the largest exchange current density (smallest charge transfer overpotential compared to the 0.36M system), the primary source of this slow decay is then attributed to slow mass transfer. When the current ceases, so does the generation of bubbles, implying the sole driving force for convection is the gradient in solution density between the surface of the electrode and the bulk solution. Assuming that the gradient in solution density is dominated by the depletion of OH⁻ ions, whose gradient is determined and fixed by the current density at the surface of the electrode, then the relative difference in density, $(\rho_{\text{bulk}} - \rho_{\text{surface}}) / \rho_{\text{bulk}}$, is smaller for 3.6M KOH at any given current density. This point is further validated by the fact that for either electrolyte, the potential decay back to OCP is consistently fastest at larger current densities. This hypothesis was further tested in the molten salt system as CER exhibits negligible charge transfer overpotential. Just like in the aqueous cases, the potential relaxes to open circuit conditions faster in the case of higher current density, as is revealed in Figure 7. This observation correlates well with the enhanced stirring observed in the high current density case (larger bubble evolution rate). The convection within the electrolyte took much longer to cease after the high current density measurements. The results in this high temperature case further evi-

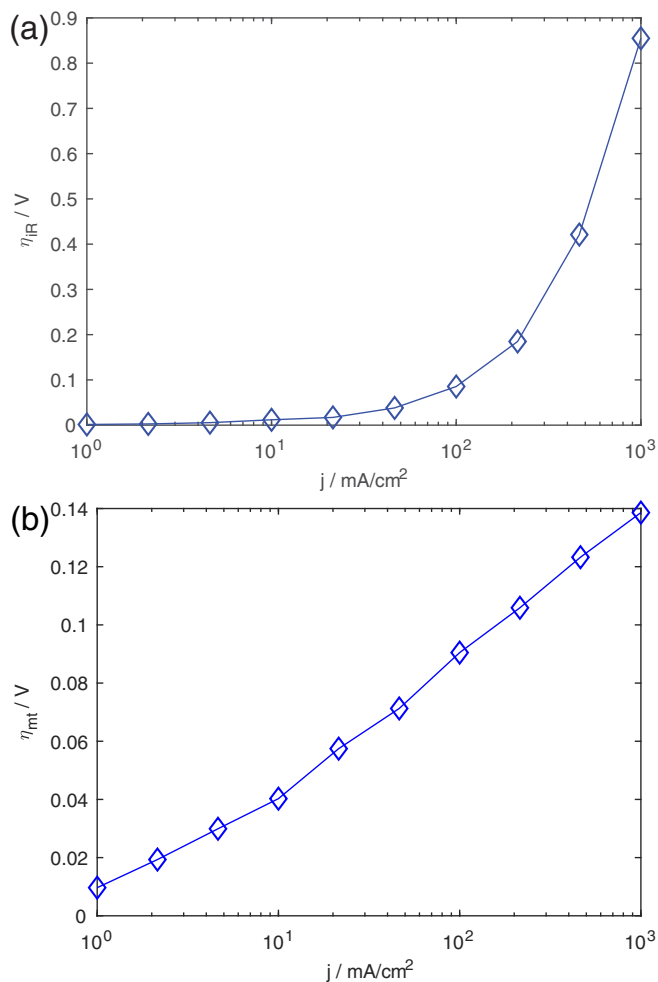


Figure 8. Ohmic (a) and mass transfer (b) overpotential variations with current density during Cl₂ evolution on glassy carbon in the molten salt electrolyte.

dence that mass transfer acts as the restoring force to reestablish the open circuit potential. The observation that the potential decayed to OCP faster in the molten salt case may be explained by the fact that Cl₂ bubbles remained attached to the glassy carbon surface long after the current was interrupted. A picture of the adhering bubbles before and after a current density of 100 mA/cm² was interrupted is shown in Figure 9 for both OER and CER. The bubbles are around 10 to 20 times larger in the case of CER and remain on the electrode for more than 10s after current interruption. For OER, the oxygen bubbles almost immediately vacate the electrode surface. The presence of these bubbles for CER offers a second mode of mass transport (in addition to convection) away from the electrode surface, allowing evaporation of dissolved chlorine molecules into the gas bubbles themselves. In the case of OER, the gas bubbles were observed to leave the electrode surface almost immediately after the current was interrupted, thus dissolved oxygen can only be subject to convection away from the electrode surface. Having used EIS to accurately determine solution resistance and charge transfer resistance, the remaining overpotential that is present can be attributed to mass transfer overpotential. Figure 10 indicates that as expected, under low to moderate current densities, charge transfer limitations dominates the overpotential behavior. However, as the current density increases and reaches industrially relevant values, the ohmic and mass transfer overpotentials become increasingly important and in the lower conductivity case, even approach (in the case of mass transfer) and overtake (in the case of ohmic losses) charge transfer kinetic as the greatest source of overpotential. Presently, the quantity assigned to η_{mt} is the sum of multiple mass transfer overpotentials

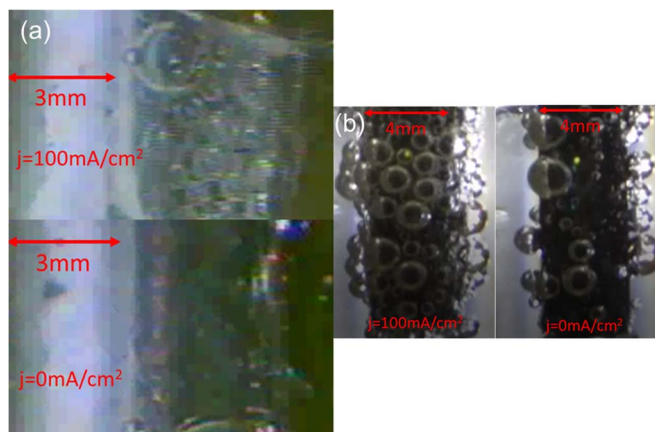


Figure 9. (a) Time lapse of oxygen bubbles evolving from Ni anode during electrolysis ($j = 100 \text{ mA/cm}^2$) and an almost complete disappearance of bubbles after the current is interrupted ($j = 0 \text{ mA/cm}^2$). (b) Time lapse of chlorine bubbles evolving from glassy carbon anode during electrolysis ($j = 100 \text{ mA/cm}^2$) and a high retainment of bubbles after the current is interrupted ($j = 0 \text{ mA/cm}^2$).

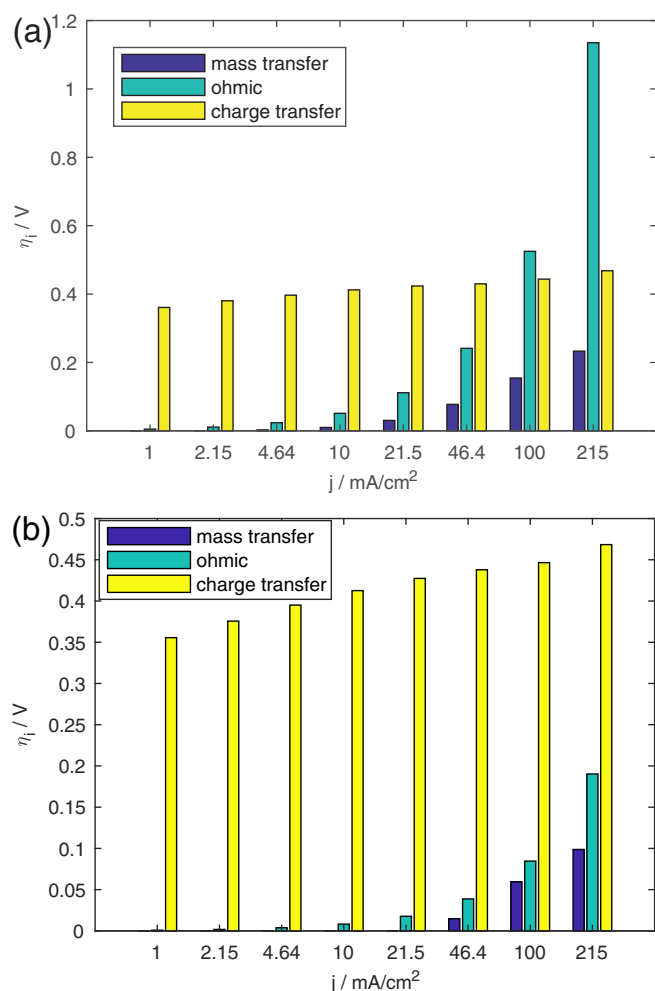


Figure 10. Overpotential contributions during OER in 0.36M KOH (a) and 3.6M KOH (b). Relative positioning of the reference electrode was within $\sim 1 \text{ mm}$ between the two studies, so differences in the ohmic overpotential are largely due to conductivity differences.

(i.e. $\eta_{OH^-,mt} + \eta_{O_2,mt}$). To further resolve the relative contributions of OH^- and O_2 transport would require varying the gas partial pressure and/or electrolyte concentration over a wider range. Interestingly, in the high temperature molten salt case, η_{mt} , which is expected to only depend on the mass transfer of Cl_2 , is the same order of magnitude as in the aqueous case, but roughly half the value.

Conclusions

The current interrupt technique has previously been applied to simple redox reaction cases with facile charge transfer kinetics to determine ohmic overpotential and mass transfer overpotentials. In this present case, solution resistance and charge transfer resistance have been measured separately using EIS. These resistance results are then applied to the potential decay curve to determine the mass transfer overpotential contribution to the total potential. In the case of a eutectic chloride electrolyte, the mass transfer overpotential associated with anodic evolution of chlorine was found to be $\sim 50\%$ lower than the low temperature anodic evolution of oxygen in alkaline electrolyte. Translating the mass transfer overpotential in terms of supersaturation of the evolved gas, CER experienced a lower degree of supersaturation than OER. This finding was supported by video evidence of larger bubbles at the surface of the electrode during CER than in OER, the bubble size being a proxy for excess chemical potential (supersaturation). The need to further refine the mass transfer overpotentials at higher current densities has been identified.

Acknowledgments

The authors acknowledge the Japanese Society for the Promotion of Science (JSPS)/NSF for enabling the experimental activities and collaboration between Japan and USA. Funding from the Office of Naval Research ONR (contract N00014-12-1-0521) to support BC is acknowledged.

List of Symbols

$a_{i,app}$	activity of species i under applied current
$a_{i,eq}$	activity of species i under equilibrium conditions
C_{dl}	double layer capacitance
CE	counter electrode
CER	chlorine evolution reaction
CI	current interrupt
E^0	standard reduction potential
E_{app}	potential under applied current
E_{eq}	equilibrium (Nernst) potential
EIS	electrochemical impedance spectroscopy
F	Faraday's constant
I	current
i_o	steady state current
J	current density
n_e	number of electrons exchanged
OER	oxygen evolution reaction
R	universal gas constant
RE	reference electrode
R_s	total solution resistance
T	absolute temperature
WE	working electrode
Z_w	Warburg impedance

Greek

η_{ct}	charge transfer overpotential
η_{IR}	ohmic overpotential
η_{mt}	mass transfer overpotential
η_{tot}	total overpotential

ORCID

Toshiyuki Nohira  <https://orcid.org/0000-0002-4053-554X>
 Takayuki Homma  <https://orcid.org/0000-0002-8279-0223>
 Antoine Allanore  <https://orcid.org/0000-0002-2594-0264>

References

1. H. Vogt and K. Stephan, *Electrochim. Acta*, **155**, 348 (2015).
2. H. Vogt, *Electrochim. Acta*, **78**, 183 (2012).
3. H. Vogt and R. J. Balzer, *Electrochim. Acta*, **50**, 2073 (2005).
4. W. Haupin and H. Kvande, *Light Met. 2000 (Ed. R.D. Peterson), Miner. Met. Mater. Soc.*, **379–384** (2000).
5. W. Botter and O. Teschke, *J. Electrochem. Soc.*, **138**, 1028 (1991).
6. J. Balej, *Int. J. Hydrogen Energy*, **10**, 233 (1985).
7. T. Kasajima, T. Nishikiori, T. Nohira, and Y. Ito, *J. Electrochem. Soc.*, **151**, E335 (2004).
8. H. Vogt, *Electrochim. Acta*, **25**, 527 (1980).
9. H. Matsushima, D. Kiuchi, and Y. Fukunaka, *Electrochim. Acta*, **54**, 5858 (2009).
10. S. Shibata, *Electrochim. Acta*, **23**, 619 (1978).
11. S. Shibata, *Bull. Chem. Soc. Jpn.*, **36**, 53 (1963).
12. S. Shibata, *Bull. Chem. Soc. Jpn.*, **33**, 1635 (1960).
13. S. Shibata, *Denki Kagaku*, **44**, 709 (1976).
14. A. El Din, *Electrochim. Acta*, **4**, 242 (1961).
15. I. G. Murgulescu, S. Sternberg, L. Medintev, and C. Mustetea, *Electrochim. Acta*, **8**, 65 (1963).
16. D. Kiuchi, H. Matsushima, Y. Fukunaka, and K. Kuribayashi, *J. Electrochem. Soc.*, **153**, E138 (2006).
17. H. Matsushima, T. Iida, and Y. Fukunaka, *J. Solid State Electrochem.*, **16**, 617 (2012).
18. J. A. Leistra, *J. Electrochem. Soc.*, **134**, 2442 (1987).
19. R. F. Scarr, *J. Electrochem. Soc.*, **116**, 1526 (1969).
20. A. J. Bard and L. R. Faulkner, *Electrochemical Methods Fundamentals and Applications*, 2nd ed., p. 833, John Wiley & Sons, Inc., New York, (2001).